



Synergistically catalytic oxidation of toluene over Mn modified g-C₃N₄/ZSM-4 under vacuum UV irradiation

Dehua Xia^{a,b,c,*}, Wenjun Xu^a, Lingling Hu^a, Chun He^a, Dennis Y.C. Leung^c, Wanjun Wang^d, Po Keung Wong^{b,*}

^a School of Environmental Science and Engineering, Sun Yat-sen University, Guangzhou, 510275, China

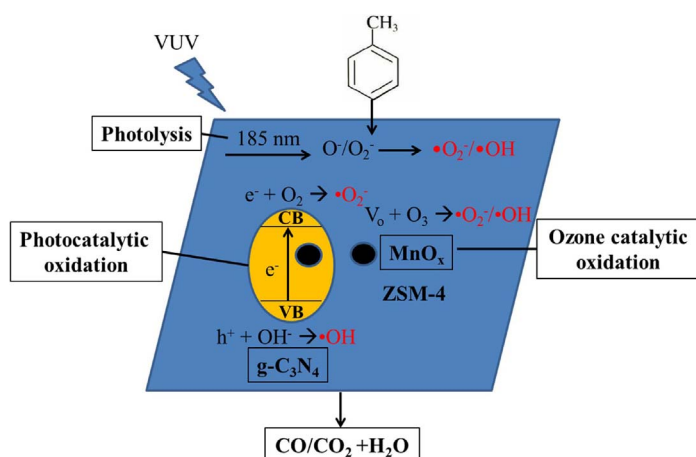
^b School of Life Sciences, The Chinese University of Hong Kong, Hong Kong SAR, Shatin, NT, China

^c Department of Mechanical Engineering, The University of Hong Kong, Hong Kong SAR, Pokfulam Road, China

^d Institute of Environmental Health and Pollution Control, School of Environmental Science and Engineering, Guangdong University of Technology, Guangzhou 510006, Guangdong, China



GRAPHICAL ABSTRACT



ARTICLE INFO

Keywords:

Mn/g-C₃N₄/ZSM-4

Multi-functional photocatalyst

VUV irradiation

O₃ Elimination

VOCs degradation

ABSTRACT

The process of vacuum ultraviolet (VUV)-assisted photocatalytic oxidation (PCO) has attracted great interest for volatile organic compounds (VOCs) degradation owing to its strong oxidation capability. However, the O₃ by-product from VUV irradiation causes secondary pollution and needs to be overcome. In this study, a multi-functional photocatalyst of Mn/g-C₃N₄/ZSM-4 was thus developed by a one-pot hydrothermal method, and then combined with VUV irradiation to eliminate O₃ byproduct as well as enhance toluene degradation via ozone-assisted catalytic oxidation (OZCO). Under VUV irradiation alone, 64% of toluene degradation was occurred but 51 ppm of O₃ was residual. In contrast, toluene degradation was enhanced to 96% over the Mn/g-C₃N₄/ZSM-4 while residual O₃ was decreased to 4 ppm. The enhanced performance was attributed to the synergistic PCO and OZCO, as the Mn modification can efficiently enhance the photocatalytic activity of g-C₃N₄ and trigger the catalytic ozonation simultaneously. The results of electron spin resonance (ESR) confirmed the generation of reactive species such as ·OH and ·O₂⁻ by VUV irradiation and then greatly enhanced after Mn/g-C₃N₄/ZSM-4 was added. Moreover, the possible mechanism of toluene degradation was also revealed through monitoring of

Abbreviations: ESR, electron spin resonance; OZCO, ozone-assisted catalytic oxidation; PCO, photocatalytic oxidation; VUV, vacuum ultraviolet; VOCs, volatile organic compounds

* Corresponding authors.

E-mail addresses: xiadehua3@mail.sysu.edu.cn (D. Xia), pkwong@cuhk.edu.hk (P.K. Wong).

<https://doi.org/10.1016/j.jhazmat.2018.01.048>

Received 28 August 2017; Received in revised form 16 January 2018; Accepted 22 January 2018

Available online 06 February 2018

0304-3894/ © 2018 Elsevier B.V. All rights reserved.

reaction intermediate. Obviously, the process of Mn/g-C₃N₄/ZSM-4 cooperated well with VUV is promising for VOCs degradation.

1. Introduction

In recent decades, China came across serious haze pollution due to industrial pollution. As one of the vital precursors to the haze pollution, the emission of volatile organic compounds (VOCs) should be strictly controlled [1]. Besides the risk of atmospheric environment, many VOCs, such as toluene, benzene and formaldehyde, are also detrimental to the public health [2,3]. To remove these hazardous VOCs, different methods have been developed and tested, including absorption [4], biological degradation [5], plasma-catalysis [6], catalytic combustion [7], and photocatalytic oxidation (PCO) [8]. Among them, PCO is a promising technology for VOCs degradation at low-concentrations due to its low cost and good oxidation ability under mild conditions [9]. However, its application still faces many problems like photocatalysts were easily deactivated and became low-efficient, causing by the residual intermediates on the surface of photocatalyst [10]. Therefore, many efforts have been made to further enhance its photocatalytic activity and stability like doping widely used TiO₂ [11,12] and developing other novel photocatalysts like perovskites, BiVO₄, g-C₃N₄ and ZnS quantum dots, etc. [13–17].

Generally, most PCO process for VOCs degradation was conducted under ultraviolet (UV) or visible light irradiation [18]. To further enhance the performance of PCO, vacuum ultraviolet (VUV) was introduced and found to be an efficient alternative for VOCs degradation, since VUV lamp can generate mercury resonance lines at both 254 nm and 185 nm to improve the light irradiation intensity [19]. The photons of 185 nm UV light can activate oxygen and water molecular to form powerful reactive species such as O(¹D), O(³P), hydroxyl radicals (·OH) and O₃ [20]. These reactive species can efficiently decompose organic intermediates and reduce their accumulation on the surface of photocatalyst, resulting in a high photocatalytic activity and stability. However, the residual O₃ from VUV irradiation can cause secondary pollution, which can cause headaches, throat inflammation, and mucosal damage [21]. To solve these problems simultaneously, Huang et al. reported a VUV-PCO process to utilize multi-functional Mn/TiO₂/ZSM-5 for benzene degradation [22,23]. This process with Mn/TiO₂/ZSM-5 can maintain its photocatalytic activity by VUV-TiO₂, as well as utilize and eliminate residual O₃ by Mn induced catalytic ozonation, leading to a higher benzene removal efficiency and lower emission of O₃ than that of TiO₂/ZSM-5. Motivated by this work, it is highly desirable to develop other novel photocatalysts with superior capacity in the VUV-PCO process.

Among recent reported photocatalysts, the simple g-C₃N₄ is much more promising for practical application, because it has unique advantages of simple structure, low costs, facile synthesis and easy to scale

up for commercial applications [24]. g-C₃N₄ has also been used in photocatalytic removal of VOCs like NO_x in air and exhibited high activity under visible light irradiation [16]. However, there is no report mentioned its photocatalytic activity under VUV irradiation. Herein, a novel photocatalyst of Mn/g-C₃N₄/ZSM-4 with multi-functions was developed by a hydrothermal method, in which Mn and g-C₃N₄ were in-situ grown on molecular sieve of ZSM-4 and then utilized to catalytic oxidation of toluene under VUV irradiation. Toluene is a kind of representative VOCs with high toxicity and photochemical activity [25]. However, many issues are still not well understood of this VUV-PCO process and deserve further investigation for application: (1) besides catalytic ozonation, the Mn modification may include other functions like enhancing photocatalytic activity of photocatalysts; (2) the generated reactive species by VUV irradiation hasn't been directly identified and may vary after photocatalysts was added; (3) the mechanism of toluene degradation hasn't been well identified in VUV-PCO process. In this work, the as-prepared Mn/g-C₃N₄/ZSM-4 are characterized by some physical and chemical techniques, and their catalytic performance for toluene oxidation was evaluated. This work may provide an efficient photocatalysts with multi-functions to surpass the conventional photocatalytic process and benefit their potential application.

2. Experimental section

2.1. Synthesis of Mn/g-C₃N₄/ZSM-4

Mn/g-C₃N₄/ZSM-4 was prepared by an in situ hydrothermal method, as shown in Fig. 1. In a typical process, 0.134 g of manganese acetate, 20 g of dicyandiamide powder and 50 mL of distilled water were put into the alumina crucible and stirred for 15 min. The molecular sieve (ZSM-4) was then immersed in the alumina crucible with above manganese acetate and dicyandiamide solution. The crucible was transferred to an oven and dried at 80 °C for 10 h to recrystallize dicyandiamide. The crucible with a cover was put into a muffle furnace and then heated for 2 h at a certain temperature with a heating rate of 15 °C/min in static air. g-C₃N₄/ZSM-4 was prepared similarly except without the addition of Mn source.

2.2. Sample characterization

UV-Vis diffuse-reflectance spectra (UV-vis DRS) of the Mn/g-C₃N₄/ZSM-4 were recorded on a Solid Spec-3700 DUV spectrophotometer using BaSO₄ as reference. The powder X-ray diffraction (XRD) patterns of the Mn/g-C₃N₄/ZSM-4 were recorded on a Bruker D8 diffractometer with monochromated Cu K α radiation ($\lambda = 1.5418 \text{ \AA}$). Fluorescence

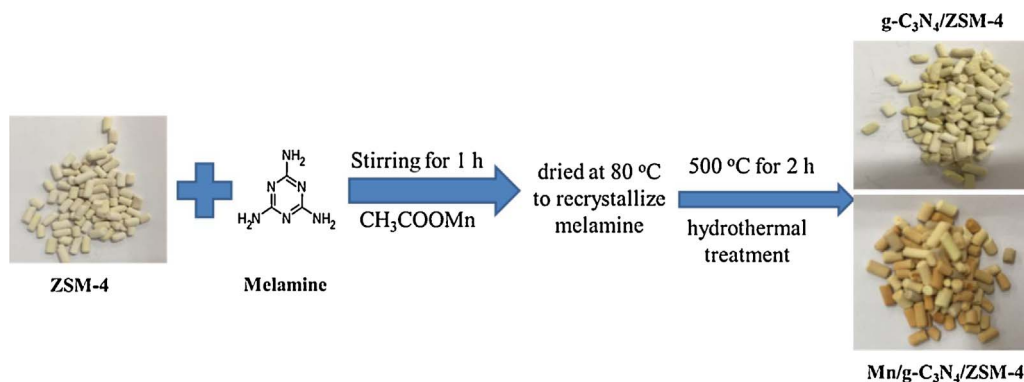


Fig. 1. The synthesis of Mn/g-C₃N₄/ZSM-4.

spectra of the Mn/g-C₃N₄/ZSM-4 were monitored with a fluorescence spectrophotometer (Hitachi, Model F-7000) equipped with a PC recorder. The morphology of the Mn/g-C₃N₄/ZSM-4 was characterized by a scanning electron microscopy with energy dispersive X-ray spectroscopy (FESEM-EDX, FEI, Quanta 400 FEG) and a transmission electron microscope (TEM, JEOL JSM-6700F).

2.3. VUV-PCO process

The schematic diagram of the VUV-PCO setup was shown in Fig. 2. A quartz tube was surrounded by two VUV lamps (4 w), which was fixed to load as-prepared photocatalyst. The gas generated from the zero air generator is dry and free of CO and CO₂. It was used to bubble water and toluene liquid to generate water and toluene vapor, respectively. The toluene concentration, humidity and gas flow were regulated by three mass flow controllers (S49, Horibametron). The concentrations of toluene, generated CO and CO₂ were measured by gas chromatography (GC) (9790II, Fuli) equipped with two flame-ionization detectors (FID). One FID was used for toluene analysis, in which the temperature of injection and detector were set at 100 °C and 250 °C, respectively. The other FID was used to determine the concentrations of CO and CO₂. The concentrations of O₃ in the inlet and outlet were monitored by an ozone analyzer (202, 2 B Technology). For each test, 1 g of the as-prepared photocatalysts was fixed in the reactor, then 25 ppm of toluene with a flow rate of 1 L/min and a relative humidity of 50% was also purged. During the treatment, the VUV lamps were turned on and gas samples were on-line fed to the GC by an automatic gas sampling valve. Moreover, the gaseous intermediates from toluene degradation were identified by GC-MS (GRIFFIN 460, LabTech), while the solid-phase intermediates deposited on the photocatalysts were extracted by CS₂ solution and then identified by GC-MS.

2.4. Reactive species analysis

Terephthalic acid (TA) at 0.5 mM in NaOH (2 mM) solution was used to detect the formation of ·OH through measuring the spectrum on a fluorescence spectrophotometer at an excitation wavelength of 365 nm [26]. The sample for electron spin resonance (ESR) spin trapping measurement (FLsp920, U.K.) was prepared by mixing Mn/g-C₃N₄/ZSM-4 in a 50 mM DMPO solution with methanol dispersion for DMPO-·O₂⁻ and aqueous dispersion for DMPO-·OH.

3. Results and discussion

3.1. Characterizations of as-prepared photocatalysts

As shown in Fig. 1, after deposition of g-C₃N₄, the surface of white ZSM-4 contained a layer of flaxen product. Besides, after the introduction of Mn into the g-C₃N₄ matrix, the Mn modified g-C₃N₄/ZSM-4 exhibited a brown color. The XRD patterns of the as-prepared Mn/g-

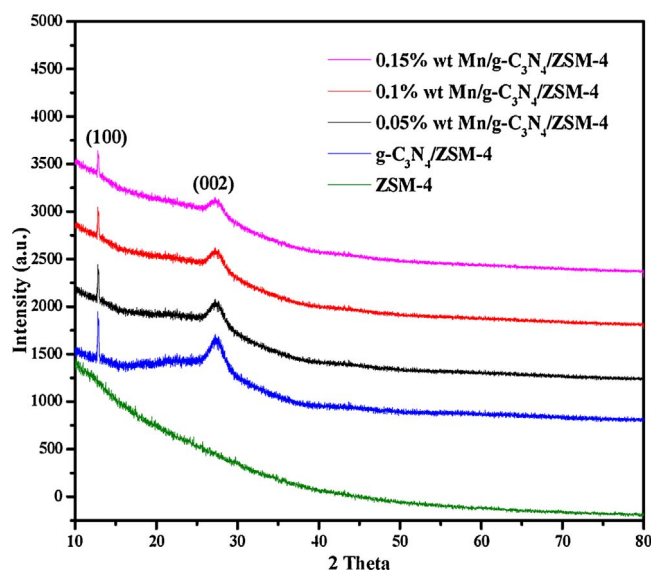


Fig. 3. XRD patterns of Mn/g-C₃N₄/ZSM-4, g-C₃N₄/ZSM-4 and ZSM-4.

C₃N₄/ZSM-4 are depicted in Fig. 3. There is no characteristic peak ascribed to the molecular sieve. After g-C₃N₄ loading, two characteristic peaks ascribed to g-C₃N₄ are obviously observed. The typical (002) interlayer stacking peak around 27.40° indicates the periodic graphitic stacking of the conjugated aromatic CN units. Another minor diffraction peak around 13.0° can be assigned to the (100) plane corresponding to the void-void distance of the in-plane structural repeating motifs [27]. After Mn modification with concentration increased from 0.05 to 0.15 wt%, there is no obvious peak corresponding to the Mn compounds like crystalline MnO₂, while g-C₃N₄ still existed in its initial phase and the diffraction peak became much weaker and widened. This is possibly ascribed to the low loading amount of the Mn element or Mn particles were in small size and well dispersed on ZSM-4.

The structure and morphology of the as-prepared photocatalysts was also investigated using SEM and shown in Fig. 4. The pristine molecular sieve contains many porous structures on the surface (Fig. 4a). In contrast, it is clearly seen that a layer of g-C₃N₄ cluster is loaded on the support surface uniformly for sample g-C₃N₄/ZSM-4. Energy dispersive X-ray (EDX) spectrum indicated the surface of g-C₃N₄/ZSM-4 co-exist the elements of C and N, with approximate 3:4 atomic ratio of C/N, confirming that crystalline g-C₃N₄ was synthesized and dispersed on ZSM-4 (Fig. 4b). After Mn deposition, little particles of Mn compounds were highly deposited on the surface. The EDX spectra also confirmed the co-existence of Mn, C and N (Fig. 4c), and the estimated molar ratio of Mn/g-C₃N₄ is 0.17. Especially, the Au and Pd in the EDX results are mainly from the preparation of specimens for SEM study.

N₂ adsorption and desorption isotherms in Fig. 5 indicate the

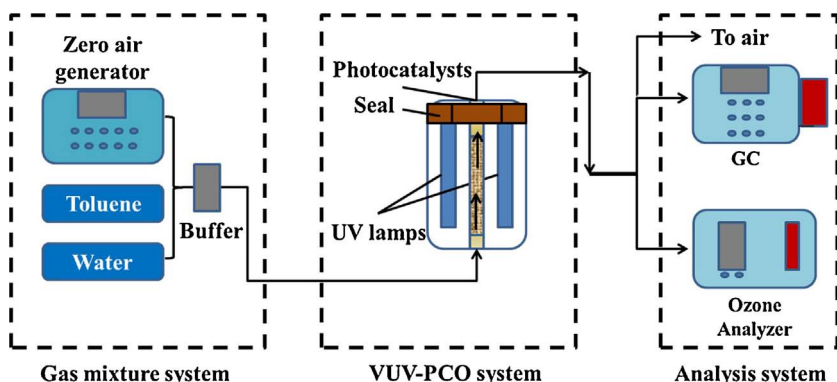


Fig. 2. The schematic diagram of VUV-PCO system.

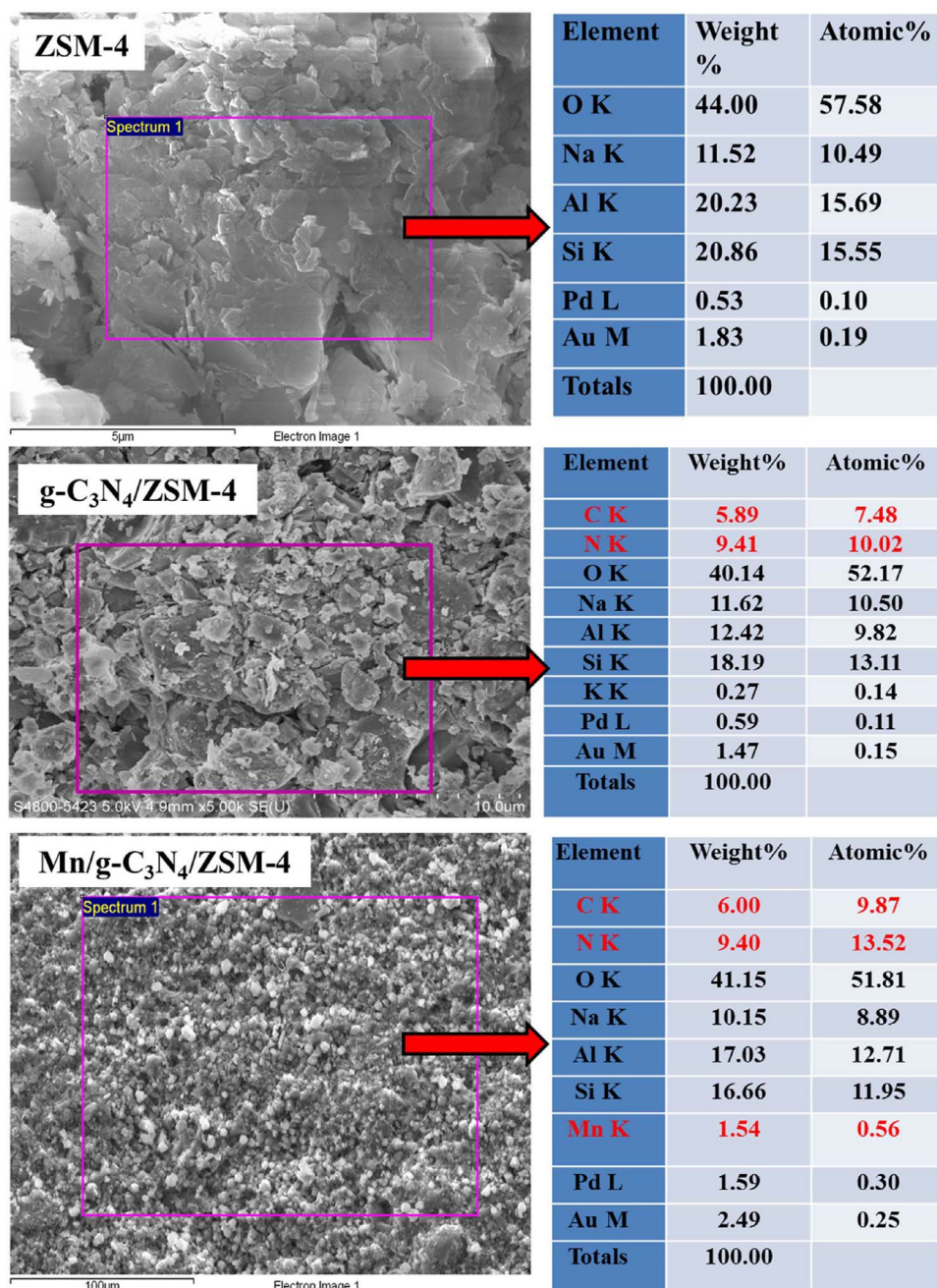


Fig. 4. SEM images of (a) ZSM-4, (b) g-C₃N₄/ZSM-4 (c) Mn/g-C₃N₄/ZSM-4.

presence of meso-pores in all the as-prepared samples. Obviously, the pore-size and specific surface area of pure ZSM-4 (3.95 nm, 0.35 cm³ g⁻¹) were greatly decreased after loading of g-C₃N₄ (3.75 nm, 0.23 cm³ g⁻¹) and even Mn modification (3.42 nm, 0.15 cm³ g⁻¹). Because the amounts of loaded g-C₃N₄ and Mn are very low in contrast with that of ZSM-4, therefore the hysteresis was almost similar for all the studied samples means ZSM-4. However, the results confirmed the fact that the surface of molecular sieve was covered by Mn particles and g-C₃N₄ polymers, as well as its pore structure was partially blocked by the Mn incorporation. This is well agreed with the results of SEM images. Generally, the porous molecular sieve provides high surface area not only for the dispersion of photocatalysts but also for the strong adsorption of toluene and ozone during the reaction.

X-ray photoelectron spectroscopy (XPS) spectra (Fig. 6) were performed to further analyze the surface chemical composition and chemical state of the as-prepared samples through scraping their surface off in advance. As shown in the survey scan XPS spectra (Fig. 6a), C 1s, N

1s and O 1s signals are observed for both samples, while Mn 2p peaks are only displayed in Mn/g-C₃N₄/ZSM-4. The existence of Mn implies the successful incorporation of Mn in g-C₃N₄ matrix. The corresponding high-resolution spectra of C 1s, N 1s, O 1s and Mn 2p are also given in Fig. 6b–d. The C 1s spectra of g-C₃N₄/ZSM-4 in Fig. 6b shows two sub-bands centered at 284.6 and 288.1 eV. The former corresponds to C–C coordination of the surface adventitious carbon while the latter is ascribed to sp³-bonded C in C–N of g-C₃N₄ [27]. The intensity of C 1s peaks centered at 284.6 eV observable for Mn/g-C₃N₄/ZSM-4 was higher than that of g-C₃N₄/ZSM-4, which can be attributed to the formation of C–O bond between C in g-C₃N₄ and O in Mn oxide after Mn hybridized with g-C₃N₄. Furthermore, the Mn/g-C₃N₄/ZSM-4 displays slightly lower binding energies of C 1s (284.6 and 288.1 eV) than g-C₃N₄/ZSM-4, further confirming that Mn has been bonded to g-C₃N₄ and the C–O bonding leads to the inner shift of C 1s [27]. These results suggest that Mn and g-C₃N₄ are not only in close linkage with each other but also form a solid Mn/g-C₃N₄ interface via C–O bonding,

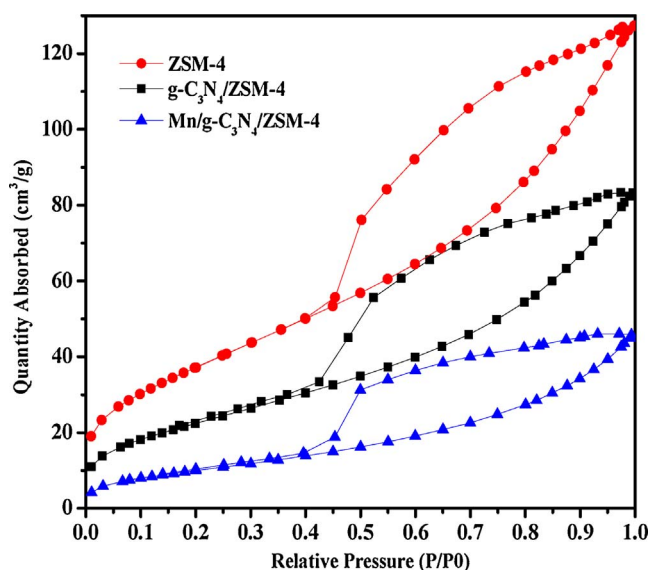


Fig. 5. N_2 adsorption and desorption curves of ZSM-4, $g-C_3N_4/ZSM-4$, $Mn/g-C_3N_4/ZSM-4$.

which will facilitate the charge transfer and separation of photo-generated carriers [28]. Fig. 6c shows the XPS N1s spectra of both $g-C_3N_4/ZSM-4$ and $Mn/g-C_3N_4/ZSM-4$. The dominated peak at 398.5 eV can be ascribed to sp^2 hybridized aromatic N bonded to carbon (C–N–C), while the peak at 399.8 eV is assigned to the tertiary N bonded to carbon atoms in the form of N–(C)3 and the peak at 401.3 eV is ascribed to amino function groups (C–N–H). Especially, there is a weakest peak at 404.3 eV (π -excitations) of N only observed in $g-C_3N_4/ZSM-4$ rather than $Mn/g-C_3N_4/ZSM-4$, implying that Mn covered up the π -excitations and coupled with $g-C_3N_4$ via an interaction using π -electrons of CN heterocycles. The high-resolution spectra of O 1s are shown in Fig. 6d, where three sub-bands can be found, the one at 529.5 eV belongs to lattice oxygen (Mn–O–Mn) in Mn, while the other two peaks at 530 and 530.9 eV are for the surface adsorbed oxygen species like hydroxide ions and water molecules, respectively [29]. Obviously, the amount of surface adsorbed oxygen species in $Mn/g-C_3N_4/ZSM-4$ has largely increased after the incorporation of Mn, making toluene molecular easily adsorbed and reacted on the catalyst surface [30]. Moreover, the high resolution Mn 2p XPS spectra of $Mn/g-C_3N_4/ZSM-4$ is also shown in Fig. 6e, in which the Mn 2p3/2 can be deconvoluted into Mn^{2+} , Mn^{3+} and Mn^{4+} sub-bands at 641 eV, 642 eV and 644 eV [31], respectively. In general, the increase of surface Mn at low valence state (Mn^{2+} , Mn^{3+}) can improve the amount of crystalline defects and oxygen vacancies, which facilitates the generation of activated oxygen species and benefit the catalytic ozonation [29].

Fig. 7 presents the UV–vis spectra of the as-prepared photocatalysts. Molecular sieve only exhibited limited light adsorption in both UV and VL region. In contrast, the $g-C_3N_4/ZSM-4$ has much stronger absorbance in the 200–450 nm regions, revealing that it has better absorption of both UV and VL. After Mn deposition, the absorption edge of $Mn/g-C_3N_4/ZSM-4$ is significantly shifted to wider wavelength regions (red shift), indicating Mn can further enhance the visible light adsorption of $g-C_3N_4/ZSM-4$. The transitions in the visible region can be assigned to Mn^{3+}/Mn^{4+} ions which have migrated into the $g-C_3N_4$ framework due to the d-orbital splitting of Mn in the doped $g-C_3N_4$ [30]. With the formation of a Mn^{4+}/Mn^{3+} dopant, energy levels are below the bottom of conduction band of $g-C_3N_4$, and in order to maintain charge neutrality, oxygen vacancies may be generated by doping of Mn^{3+} in the lattice. Based on the Kubelka-Munk transformation, $ah\nu = A(h\nu - E_g)^n/2$ [31], the band energy for $Mn/g-C_3N_4/ZSM-4$ was calculated to be 2.65 eV.

In order to analyze the generation, separation and migration

efficiency of photogenerated carriers in $Mn/g-C_3N_4/ZSM-4$, photoelectrochemical measurements were performed. Fig. 8 shows the typical I–t curves for as-prepared electrodes of $Mn/g-C_3N_4/ZSM-4$ with several on-off cycles of intermittent VUV irradiation at a constant bias of 0.1 V vs. SCE with the measured solution pH of 7.4. After hybridization with Mn, the photocurrent of $Mn/g-C_3N_4/ZSM-4$ is much enhanced compared to that of $g-C_3N_4/ZSM-4$, indicating the largely lowered recombination rate and efficiently promoted separation of photogenerated carriers. Multiple valences of Mn ions benefit the charges transfer in $g-C_3N_4$ [32]. Moreover, Mn oxide is a narrow band semiconductor, which can form a composite with $g-C_3N_4$, also can accelerate the separation of electron-hole in $g-C_3N_4$ [33]. Moreover, the photocurrent increases sharply when the light is switched on, and immediately returns to its initial state after the light source is turned off, which is repeatable. This result indicates $Mn/g-C_3N_4/ZSM-4$ has an efficient electron-hole separation and good structural stability.

3.2. Toluene degradation and mineralization by VUV-PCO system

The performance of toluene degradation under different processes was compared under UV/VUV irradiation and the results were shown in Fig. 9. Bare molecular sieve of ZSM-4 exhibited some adsorption in the initial 10 min and then attained equilibration with less than 10% toluene removal. Under UV irradiation, $Mn/g-C_3N_4/ZSM-4$ (18%) exhibited a little enhanced photocatalytic performance than $g-C_3N_4/ZSM-4$ (15%) towards toluene oxidation, consistent with higher photocurrent of $Mn/g-C_3N_4/ZSM-4$ in Fig. 8. In contrast, it is interesting to find that VUV-PCO process achieved much higher toluene removal efficiency than conventional UV-PCO process. Under VUV irradiation, toluene removal efficiency increased in the order of VUV photolysis < ZSM-4 < $g-C_3N_4/ZSM-4$ < $Mn/g-C_3N_4/ZSM-4$. With VUV alone, it was stably maintained at about 64% for the whole VUV photolysis. When bare molecular sieve was combined with the VUV photolysis, toluene removal efficiency was little increased to 67%. This suggested that toluene degradation was mainly ascribed to the VUV photolysis, because bare molecular sieve only exhibited limited adsorption to improve toluene degradation. In contrast, after the loading of $g-C_3N_4$ over ZSM-4, toluene removal efficiency was enhanced to 78% in the VUV-PCO process, indicating $g-C_3N_4/ZSM-4$ exhibits good photocatalytic activity under VUV irradiation. As for $Mn/g-C_3N_4/ZSM-4$, it achieved the best performance with toluene removal efficiency stably kept at 96%. It is even superior to the sum of VUV photolysis and PCO, indicating that more degradation pathways were involved for toluene oxidation. Based on Huang et al.'s work [34], it is suggested that the toluene after VUV photolysis and PCO further underwent catalytic oxidation in the ozone-assisted catalytic oxidation (OZCO) unit, due to the catalysts well synergized with VUV irradiation. Moreover, the enhanced photocatalytic activity after Mn doping with $g-C_3N_4$ also plays an important role for enhanced toluene degradation. Moreover, the kinetics of the degradation of toluene was described by the pseudo first-order rate equation within the initial 10 min. As shown in Table 1, the $Mn/g-C_3N_4/ZSM-4$ sample under VUV irradiation ($k = 0.274 \text{ min}^{-1}$) exhibited the best photocatalytic activity among the samples. Meanwhile, the changes of GC peak during toluene degradation with $Mn/g-C_3N_4/ZSM-4$ under VUV irradiation were shown in Fig. S1 and Table S1.

In order to confirm the mineralization of toluene in the process, the COx concentrations in the outlet stream was measured. Fig. 10 shows the concentration of CO or CO_2 generated from toluene degradation under different processes. For the bare molecular sieve, the outlet CO and CO_2 reached 36 and 51 ppm, respectively, which was close to that of the VUV photolysis (35 ppm of CO and 48 ppm of CO_2). These results further confirmed that the toluene degradation is mainly attributed to the VUV photolysis. As for the VUV-PCO reaction with $g-C_3N_4/ZSM-4$, CO concentration (31 ppm) was lower than that of the VUV photolysis (35 ppm), while CO_2 concentrations greatly increased from 48 ppm to

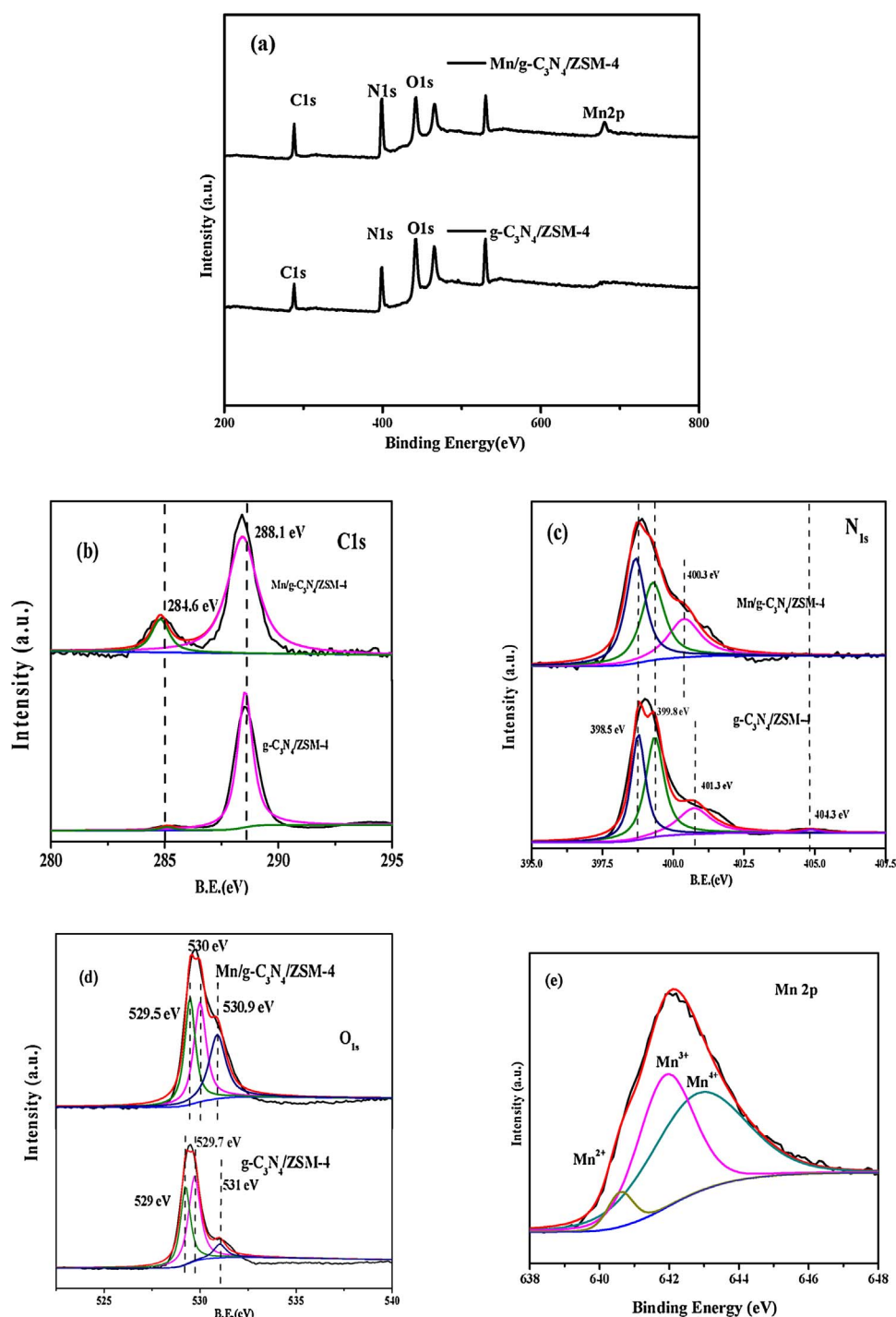


Fig. 6. (a) XPS spectra of g-C₃N₄/ZSM-4 and Mn/g-C₃N₄/ZSM-4; high resolution XPS spectra of the element (b) C, (c) N, (d) O and (e) Mn in g-C₃N₄/ZSM-4 and Mn/g-C₃N₄/ZSM-4.

54 ppm. This result indicates the residual toluene from the VUV photolysis can be further oxidized into CO₂ by PCO with the g-C₃N₄/ZSM-4, leading to the better toluene mineralization. Obviously, bare molecular sieve can hardly promote toluene degradation, but the loading of g-C₃N₄ on ZSM-4 significantly improved the removal efficiency and mineralization rate of toluene. Moreover, the CO₂ concentration further reached to 69 ppm and CO concentration decreased to 11 ppm over the Mn/g-C₃N₄/ZSM-4 under VUV irradiation, indicating that the Mn doping over g-C₃N₄/ZSM-4 greatly enhanced toluene degradation and mineralization. Obviously, its CO₂ concentration is also larger than the sum of that of VUV photolysis and PCO alone, in accordance with toluene removal efficiency in Fig. 9. The enhanced toluene removal was attributed to the synergistic effect of PCO-VUV and Mn should be one of

the primary active centers.

In order to analyze the role of O₃ on toluene oxidation, the residual O₃ concentration over different catalysts was monitored, which is following the order: Mn/g-C₃N₄/ZSM-4 (4 ppm) < g-C₃N₄/ZSM-4 (38 ppm) < ZSM-4 (47 ppm) ≈ VUV photolysis (51 ppm) (Fig. 11). This is just opposite to that of toluene removal efficiency (Fig. 9) and CO_x concentration (Fig. 10), indicating that the residual O₃ was greatly involved in the process of toluene removal. The residual O₃ concentration over g-C₃N₄/ZSM-4 was 38 ppm, lower than VUV photolysis (51 ppm), suggesting the photocatalytic activity of g-C₃N₄/ZSM-4 has some effect for O₃ decomposition. Previous work has indicated O₃ can be efficiently decomposed into O₂ and O[•] by irradiated TiO₂, as O₃ is a good electron acceptor for PCO [35]. In contrast, Mn/g-C₃N₄/ZSM-4

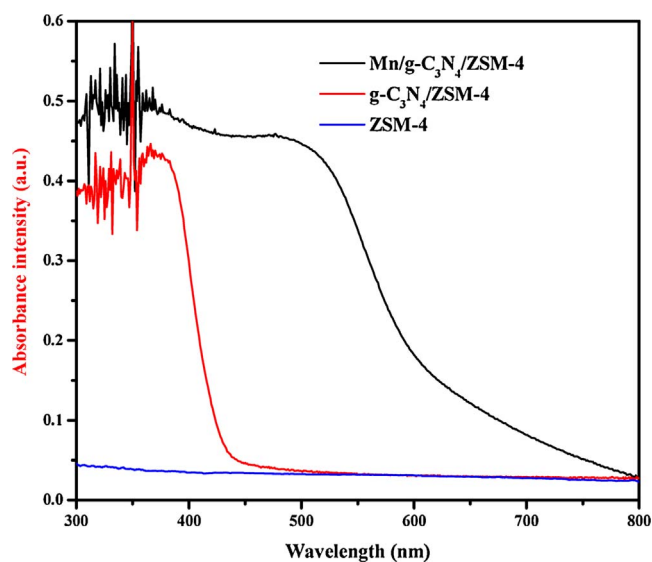


Fig. 7. UV-vis absorbance spectra of Mn/g-C₃N₄/ZSM-4, g-C₃N₄/ZSM-4, ZSM-4.

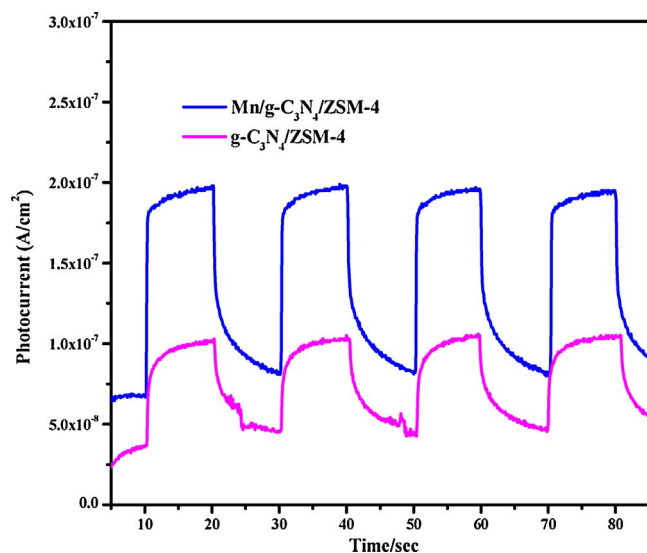


Fig. 8. Photocurrent and photoluminescence (PL) analysis of Mn/g-C₃N₄/ZSM-4 and g-C₃N₄/ZSM-4.

exhibited the best catalytic activity towards O₃, resulting in a lowest residual O₃ concentration of 4 ppm. Obviously, the Mn incorporation over g-C₃N₄/ZSM-4 greatly enhanced O₃ decomposition. This is because the Mn can provide enough active sites and has highly reactive activity towards O₃ decomposition [36]. Therefore, Mn/g-C₃N₄/ZSM-4 is well synergized with VUV irradiation to decompose O₃ and utilize it to enhance toluene degradation via ozone-assisted catalytic oxidation (OZCO). Due to the efficient catalytic ozonation of Mn/g-C₃N₄/ZSM-4, the O₃ by-product can be efficiently utilized for toluene oxidation and the photocatalyst achieved the highest removal efficiency of toluene. Moreover, it can be found that the catalytic/photocatalytic stability could be maintained throughout the measurement.

3.3. Scheme of degradation and mineralization by VUV-PCO

In contrast with conventional PCO process, the synergistic effect of more pathways efficiently destructed the toluene, including VUV photolysis, PCO and OZCO for Mn/g-C₃N₄/ZSM-4 under VUV irradiation. Obviously, VUV photolysis played a critical role for toluene degradation with 64% of toluene removal. As for PCO, 254 nm rather than 185 nm

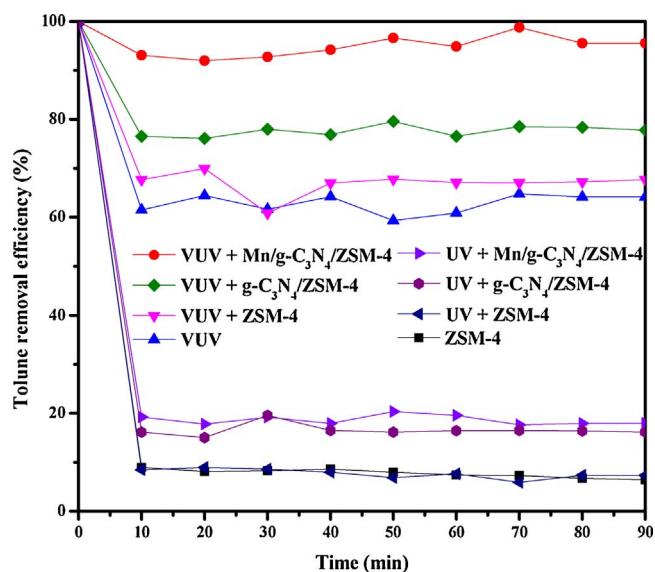


Fig. 9. Toluene removal efficiency of different catalysts under VUV and UV irradiation.

Table 1
Comparison of the rate constants for the photocatalytic removal of toluene at different conditions.

Sample	Pseudo-first order rate constant (min ⁻¹)	
	UV	VUV
No catalyst	0.0015	0.205
ZSM-4	0.0022	0.208
g-C ₃ N ₄ /ZSM-4	0.0029	0.221
Mn/g-C ₃ N ₄ /ZSM-4	0.0034	0.274

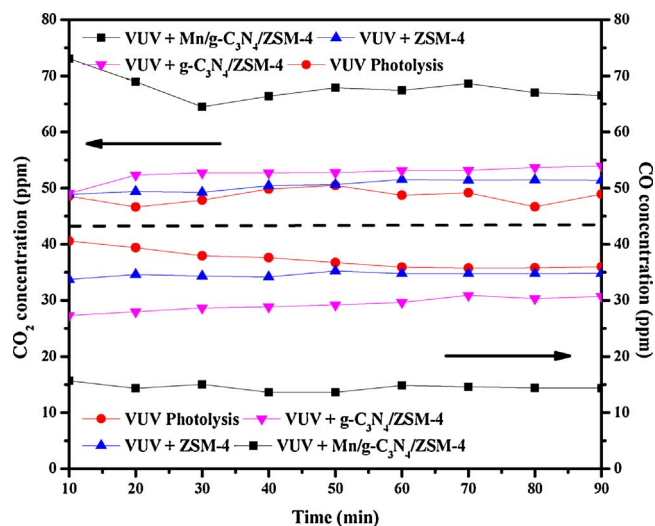


Fig. 10. Outlet CO_x concentration of different catalysts under VUV irradiation.

of VUV irradiation can be primarily utilized to activate the g-C₃N₄ for PCO. This is because the emission intensity at 185 nm constitutes only 8% of VUV irradiation and it is seriously decayed in air due to the strong adsorption by O₂ and moisture [37]. Through analyzing the values of photocatalytic degradation performance by these photocatalysts, it can estimate that PCO can roughly remove 14% of toluene and OZCO can remove 18% of toluene over Mn/g-C₃N₄/ZSM-4 in the VUV-PCO process. Moreover, EPR spin-trap technique with DMPO was used to directly detect the radicals in catalysts suspensions with ozone

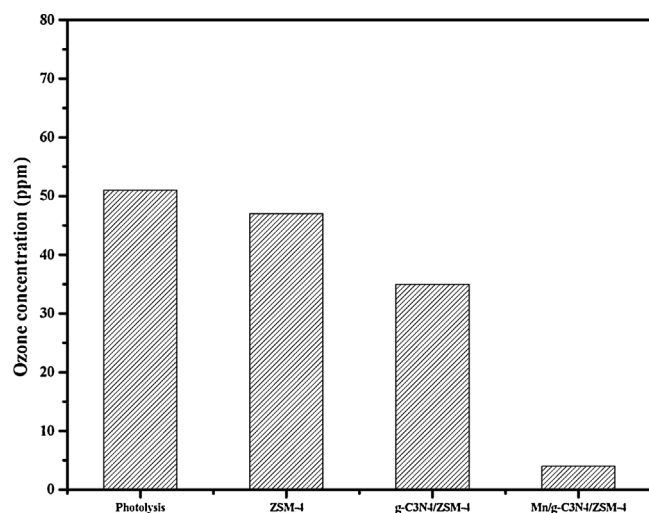
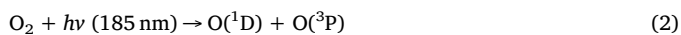


Fig. 11. Residual O₃ concentration of different catalysts under VUV irradiation.

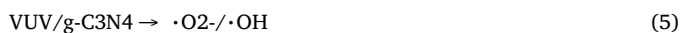
(Fig. 12). In the presence of Mn/g-C₃N₄/ZSM-4, the peak intensities of ·OH signal were higher than those ones in ozone alone solution, indicating that the adsorbed ozone on the surface was quickly decomposed into reactive oxygen species. ·O₂⁻ and ·OH is highly reactive and can efficiently enhance toluene oxidation [20–22].

The possible schematic of toluene degradation in the VUV-PCO process over Mn/g-C₃N₄/ZSM-4 is proposed in Fig. 13. First, molecular sieve contributed little to toluene degradation and O₃ decomposition, but its high surface area and suitable pore diameter showed a powerful capacity for toluene adsorption. Meanwhile, the mesoporous structure of molecular sieve also can serve as reservoirs to stock the intermediate species and residual O₃, which prolonged the treatment time and benefit for the reaction. Moreover, the Lewis acid sites of molecular sieve can react with ozone to generate surface atomic oxygen and may also contribute to the catalytic ozonation, suggested by Silva et al. [38].

Second, under VUV irradiation, energetic photons (185 nm) can directly react with absorbed oxygen to generate reactive oxygen species for toluene degradation such as ·OH via the following steps (1–4) [39,40]:



Third, g-C₃N₄ acted as the active center for the PCO of toluene. It is generally regarded that ·OH and ·O₂⁻ generated from g-C₃N₄ is responsible for the degradation of VOCs [16], well evidenced by the results of EPR analysis (Fig. 12). Meanwhile, the Mn doping also accelerated the separation of e⁻-h⁺ pairs and enhanced PCO, as shown in Fig. 8. Moreover, PCO should be also involved in catalytic decomposition of O₃ via following steps (5–7) since the introduction of g-C₃N₄ into Mn/g-C₃N₄/ZSM-4 significantly improved O₃ decomposition [35].



Fourth, Mn acted as the active center for catalytic decomposition of O₃ and OZCO of toluene. It is reported that, the catalytic ozonation is closely related to the oxygen vacancy of Mn [37]. The O₃ molecule was bound to Mn/g-C₃N₄/ZSM-4 surface by inserting an O atom into an oxygen vacancy site. The oxygen vacancy transferred 2-electron to an O

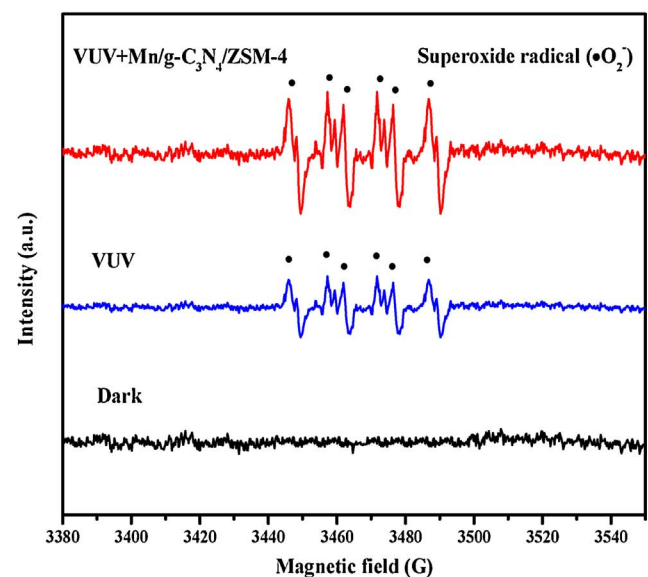
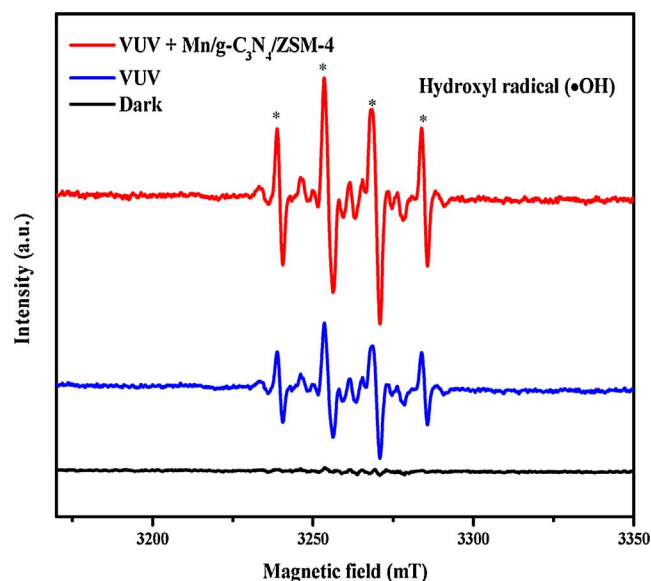


Fig. 12. Time-dependent photoluminescence spectra of a terephthalic acid solution containing Mn/g-C₃N₄/ZSM-4 under VUV irradiation.

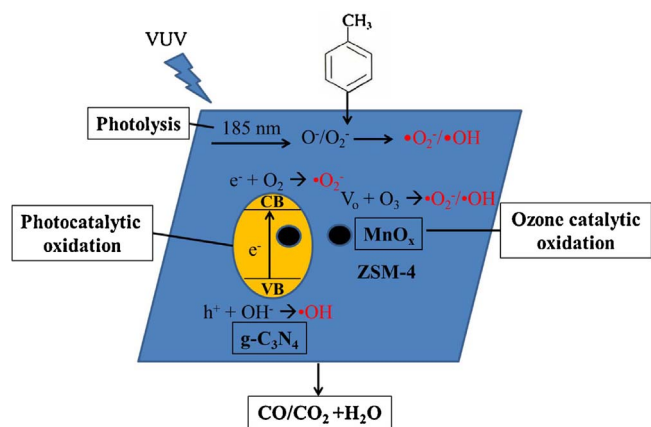


Fig. 13. The schematic of toluene oxidation in VUV-PCO process over Mn/g-C₃N₄/ZSM-4 catalyst.

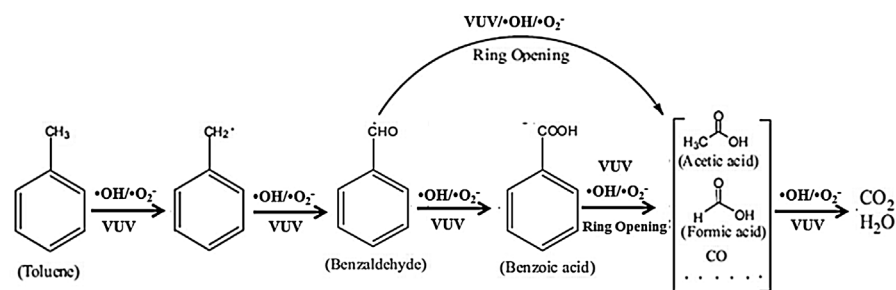
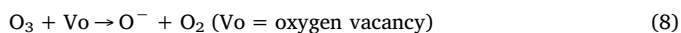


Fig. 14. Degradation process of toluene under VUV-PCO process.

Table 2
Comparison of toluene removal efficiency with other studies.

Light source	Light intensity	Catalyst	Dosage	Inlet	Pseudo-first order rate constant	References
Visible light (200 W Xenon lamp)	200 mW/cm ²	g-C ₃ N ₄ /BiVO ₄	100 mg	25 ppm	0.132 h ⁻¹	Sun et al. [44]
Visible light (300 W Xenon lamp)	220 mW/cm ²	Bi-Zn/TiO ₂	100 mg	280 ppm	0.01 min ⁻¹	Li et al. [45]
UV (25 W LED lamp)	14.5 mW/cm ²	TiO ₂ -MnO ₂ nanotubes	Not available	200 ppm	0.009 min ⁻¹	Nevárez-Martínez et al. [46]
UV (20 W UV-LED lamp)	10 mW/cm ²	TiO ₂ nanotubes	150 mg	20 ppm	0.061 min ⁻¹	Weon et al. [47]
UV (20 W UV-LED lamp)	10 mW/cm ²	TiO ₂ nanoparticles @TiO ₂ nanotubes	150 mg	20 ppm	0.105 min ⁻¹	Weon et al. [47]
UN (6 W VUV tube)	4 mW/cm ²	Mn/g-C ₃ N ₄ /ZSM-4	1 g	25 ppm	0.274 min ⁻¹	This study

atom of O₃, thus forming surface reactive oxygen species like an oxygen species (O⁻) and a bridging O₂ dimer (peroxide, O₂⁻). The O₂⁻ can further react with H₂O to generating ·OH or ·O₂⁻ for VOCs oxidation (Eqs. (8)–(10)) [41]. O₃ from VUV irradiation will be decomposed under the help of Mn catalyst, generating ·OH and ·O₂⁻ via the following steps [42]:



Therefore, ZSM-4, g-C₃N₄, and Mn well cooperate together to achieve multi-functions for the efficient removal of toluene as well as elimination of O₃ under VUV irradiation, finally the Mn/g-C₃N₄/ZSM-4 achieved efficient O₃ decomposition and toluene oxidation.

3.4. Pathway of toluene degradation under VUV-PCO process

In previous works, different mechanism and pathway of toluene degradation were proposed according to the identified intermediates [21,22]. However, the mechanism of toluene degradation hasn't been well identified in VUV-PCO process. In VUV-PCO process, the generated reactive species such as ·OH and ·O₂⁻ can flow through the reactor to take part in the catalytic oxidation. Therefore, the oxidation process of toluene not only occurred on the surface of photocatalyst but also in the bulk gas-phase. To analyze the degradation pathways, the adsorbed intermediates on catalysts (solid-phase) and gaseous intermediates (gas-phase) were investigated by GC-MS, respectively. There is limited gas-phase by-products can be detected in the GC-MS chromatograms, indicating that the gas-phase intermediates could be adsorbed on the surface of photocatalysts or degraded into environmental friendly CO₂ and H₂O. Based on the identified by-products and products, the possible pathway of toluene degradation in the VUV-PCO was proposed, as shown in Fig. 14. Through a series of process such as splitting of toluene, hydrogenation, H abstraction and ring opening by ·OH or ·O₂⁻ radicals, toluene was degraded into active acid and formic acid etc. [43]. Moreover, the intermediates are easy to be further degraded and mineralized into CO₂ and H₂O.

Moreover, Table 2 summarized the maximum toluene removal efficiencies obtained in other studies compared to the result of this study. Li et al. [45] applied Bi-Zn/TiO₂ and Nevárez-Martínez et al. [46] used

TiO₂-MnO₂ nanotubes in their VL processes, while Weon et al. [47] used TiO₂ nanotubes in their UV processes. Although the experimental conditions for each test are different, the pseudo-first order rate constant (min⁻¹) is a parameter that can be utilized for quantitative comparison. As shown in Table 2, our present system obtained a maximum rate constant, which is superior to those of other studies by about 2–3 times. Again, the Mn deposited onto g-C₃N₄, which can achieve synergistic effect of photocatalytic oxidation and ozone, exhibiting a promising application future.

4. Conclusions

A multi-functional photocatalyst of Mn/g-C₃N₄/ZSM-4 was developed by a one-pot hydrothermal method and used for toluene degradation under VUV irradiation. Both toluene and residual O₃ was efficiently removed over Mn/g-C₃N₄/ZSM-4. Mn/g-C₃N₄/ZSM-4 cooperated well with VUV irradiation for toluene degradation, leading to the high toluene removal efficiency. It includes three efficient pathways like VUV photolysis, PCO and OZCO for toluene degradation. The Mn incorporation can efficiently trigger the catalytic ozonation and enhance the photocatalytic activity of g-C₃N₄ simultaneously. The scheme of toluene degradation by VUV-PCO was proposed. This study provides an efficient catalyst for VOCs degradation.

Acknowledgements

The project was supported by a research grant (GRF14100115) of the Research Grant Council, Hong Kong SAR Government and the Technology and Business Development Fund (TBF15SCI008) of The Chinese University of Hong Kong to P.K. Wong, the research grant (41573086) of National Natural Science Foundation of China to D. Xia, and the research grant of National Natural Science Foundation of China (No. 51578556), Natural Science Foundation of Guangdong Province (No. 2015A030308005), Science and Technology Research Programs of Guangdong Province (No. 2014A020216009) to C. He, respectively. P.K. Wong was also supported by CAS/SAFEA International Partnership Program for Creative Research Teams of Chinese Academy of Sciences (2015HSC-UE004). The authors also wants to thank Muyan Wu (HKU), Huadan Liu (SYSU) and Huanjunwa He (SYSU) for their technical assistance.

Appendix A. Supplementary data

Supplementary material related to this article can be found, in the online version, at doi:<https://doi.org/10.1016/j.jhazmat.2018.01.048>.

References

- [1] R.-J. Huang, Y. Zhang, C. Bozzetti, K.-F. Ho, J.-J. Cao, Y. Han, K.R. Daellenbach, J.G. Slowik, S.M. Platt, F. Canonaco, High secondary aerosol contribution to particulate pollution during haze events in China, *Nature* 514 (2014) 218–222.
- [2] T.-D. Pham, B.-K. Lee, C.-H. Lee, The advanced removal of benzene from aerosols by photocatalytic oxidation and adsorption of Cu-TiO₂/PU under visible light irradiation, *Appl. Catal. B: Environ.* 182 (2016) 172–183.
- [3] X. Wang, Q. Ni, D. Zeng, G. Liao, C. Xie, Charge separation in branched TiO₂ nanorod array homojunction aroused by quantum effect for enhanced photocatalytic decomposition of gaseous benzene, *Appl. Surf. Sci.* 389 (2016) 165–172.
- [4] B. Ozturk, D. Yilmaz, Absorptive removal of volatile organic compounds from flue gas streams process, *Saf. Environ.* 84 (2006) 391–398.
- [5] W.H. Chen, W.B. Yang, C.S. Yuan, J.C. Yang, Q.L. Zhao, Fates of chlorinated volatile organic compounds in aerobic biological treatment processes: the effects of aeration and sludge addition, *Chemosphere* 103 (2014) 92–98.
- [6] X. Xu, P. Wang, W. Xu, J. Wu, L. Chen, M. Fu, D. Ye, Removal of toluene in adsorption-discharge plasma systems over a nickel modified SBA-15 catalyst, *Chem. Eng. J.* 283 (2016) 276–284.
- [7] S. Scirè, S. Minicò, C. Crisafulli, C. Satriano, A. Pistone, Catalytic combustion of volatile organic compounds on gold/cerium oxide catalysts, *Appl. Catal. B: Environ.* 40 (2003) 43–49.
- [8] D. Xia, L. Hu, X. Tan, C. He, W. Pan, T. Yang, Y. Huang, D. Shu, Immobilization of self-stabilized plasmonic Ag-AgI on mesoporous Al₂O₃ for efficient purification of industrial waste gas with indoor LED illumination, *Appl. Catal. B: Environ.* 185 (2016) 295–306.
- [9] D. Xia, L. Hu, C. He, W. Pan, T. Yang, Y. Yang, D. Shu, Simultaneous photocatalytic elimination of gaseous NO and SO₂ in a BiOI/Al₂O₃-padded trickling scrubber under visible light, *Chem. Eng. J.* 279 (2015) 929–938.
- [10] T. Yan, J. Long, X. Shi, D. Wang, Z. Li, X. Wang, Efficient photocatalytic degradation of volatile organic compounds by porous indium hydroxide nanocrystals, *Environ. Sci. Technol.* 44 (4) (2010) 1380–1385.
- [11] J. Mo, Y. Zhang, Q. Xu, Y. Zhu, J.J. Lamson, R. Zhao, Determination and risk assessment of by-products resulting from photocatalytic oxidation of toluene, *Appl. Catal. B: Environ.* 89 (3–4) (2009) 570–576.
- [12] M.D. Hernández-Alonso, F. Fresno, S. Suárez, J.M. Coronado, Development of alternative photocatalysts to TiO₂: challenges and opportunities, *Energy Environ. Sci.* 2 (12) (2009) 1231–1257.
- [13] J. Chen, Z. He, G. Li, T. An, H. Shi, Y. Li, Visible-light-enhanced photo-thermocatalytic activity of ABO(3)-type perovskites for the decontamination of gaseous styrene, *Appl. Catal. B: Environ.* 209 (2017) 146–154.
- [14] F. Dong, Z. Wang, Y. Li, W.-K. Ho, S.C. Lee, Immobilization of polymeric g-C₃N₄ on structured ceramic foam for efficient visible light photocatalytic air purification with real indoor illumination, *Environ. Sci. Technol.* 48 (2014) 10345–10353.
- [15] H.R. Rajabi, O. Khani, M. Shamsipur, V. Vatanpour, High-performance pure and Fe³⁺-ion doped ZnS quantum dots as green nanophotocatalysts for the removal of malachite green under UV-light irradiation, *J. Hazard. Mater.* 250–251 (2013) 370–378.
- [16] H.R. Rajabi, M. Farsi, Study of capping agent effect on the structural, optical and photocatalytic properties of zinc sulfide quantum dots, *Mater. Sci. Semiconduct. Proc.* 48 (2016) 14–22.
- [17] H.R. Rajabi, M. Farsi, Effect of transition metal ion doping on the photocatalytic activity of ZnS quantum dots: synthesis, characterization, and application for dye decolorization, *J. Mol. Catal. A: Chem.* 399 (2015) 53–61.
- [18] K. Zoschke, H. Bornick, E. Worch, Vacuum-UV radiation at 185 nm in water treatment—a review, *Water Res.* 52 (2014) 131–145.
- [19] J. Kim, P. Zhang, J. Li, J. Wang, P. Fu, Photocatalytic degradation of gaseous toluene and ozone under UV₂₅₄+185 nm irradiation using a Pd-deposited TiO₂ film, *Chem. Eng. J.* 52 (2014) 337–345.
- [20] P. Zhang, J. Liu, Z.L. Zhang, VUV photocatalytic degradation of toluene in the gas phase, *Chem. Lett.* 33 (2004) 1242–1243.
- [21] M. Sayed, P. Fu, L.A. Shah, H.M. Khan, J. Nisar, M. Ismail, P. Zhang, VUV-photocatalytic degradation of bezafibrate by hydrothermally synthesized enhanced {001} facets TiO₂/Ti film, *J. Phys. Chem. A* 120 (2016) 118–127.
- [22] J. Yuan, X. Huang, M. Chen, J. Shi, W. Shangguan, Ozone-assisted photocatalytic degradation of gaseous acetaldehyde on TiO₂/M-ZSM-5 (M = Zn, Cu, Mn), *Catal. Today* 201 (2013) 182–188.
- [23] H. Huang, H. Huang, Q. Feng, G. Liu, Y. Zhan, M. Wu, H. Lu, Y. Shu, D.Y.C. Leung, Catalytic oxidation of benzene over Mn modified TiO₂/ZSM-5 under vacuum UV irradiation, *Appl. Catal. B: Environ.* 203 (2017) 870–878.
- [24] H. Wang, Y. Su, H.X. Zhao, H.T. Yu, S. Chen, Y.B. Zhang, X. Quan, Photocatalytic oxidation of aqueous ammonia using atomic single layer graphitic-C₃N₄, *Environ. Sci. Technol.* 48 (2014) 11984–11990.
- [25] J. Jeong, K. Sekiguchi, K. Sakamoto, Photochemical and photocatalytic degradation of gaseous toluene using short-wavelength UV irradiation with TiO₂ catalyst: comparison of three UV sources, *Chemosphere* 57 (2004) 663–671.
- [26] D. Xia, Z. Shen, G. Huang, W. Wang, J. Yu, P.K. Wong, Red phosphorus: an earth-abundant elemental photocatalyst for “green” bacterial inactivation under visible light, *Environ. Sci. Technol.* 49 (2015) 6264–6273.
- [27] J. Luo, G. Dong, Y. Zhu, Z. Yang, C. Wang, Switching of semiconducting behavior from n-type to p-type induced high photocatalytic NO removal activity in g-C₃N₄, *Appl. Catal. B: Environ.* 214 (2017) 46–56.
- [28] M. Wang, M. Shen, L. Zhang, J. Tian, X. Jin, Y. Zhou, J. Shi, 2D-2D MnO₂/g-C₃N₄ heterojunction photocatalyst: *in-situ* synthesis and enhanced CO₂ reduction activity, *Carbon* 120 (2017) 23–31.
- [29] V.P. Santos, M.F.R. Pereira, J.J.M. Orfao, J.L. Figueiredo, The role of lattice oxygen on the activity of manganese oxides towards the oxidation of volatile organic compounds, *Appl. Catal. B: Environ.* 99 (2010) 353–363.
- [30] G. Dong, Z. Ai, L. Zhang, Efficient anoxic pollutant removal with oxygen functionalized graphitic carbon nitride under visible light, *RSC Adv.* 4 (2014) 5553–5560.
- [31] Z. Shu, Y. Chen, W. Huang, X. Cui, L. Zhang, H. Chen, G. Zhang, X. Fan, Y. Wang, G. Tao, He D, J. Shi, Room-temperature catalytic removal of low-concentration NO over mesoporous Fe-Mn binary oxide synthesized using a template-free approach, *Appl. Catal. B: Environ.* 140–141 (2013) 42–50.
- [32] J. Tauc, Absorption edge and internal electric fields in amorphous semiconductors, *Mater. Res. Bull.* 5 (1970) 721–729.
- [33] M. Wang, L. Zhang, W. Huang, T. Xiu, C. Zhuang, J. Shi, The catalytic oxidation removal of low-concentration HCHO at high space velocity by partially crystallized mesoporous MnOx, *Chem. Eng. J.* 320 (2017) 667–676.
- [34] H. Huang, X. Ye, W. Huang, J. Chen, Y. Xu, M. Wu, Q. Shao, Z. Peng, G. Ou, J. Shi, Ozone-catalytic oxidation of gaseous benzene over MnO₂/ZSM-5 at ambient temperature: catalytic deactivation and its suppression, *Chem. Eng. J.* 264 (2015) 24–31.
- [35] Y. Lin, C. Lin, Catalytic and photocatalytic degradation of ozone via utilization of controllable nano-Ag modified on TiO₂, *Environ. Progr.* 27 (2008) 498–502.
- [36] P. Fu, P. Zhang, J. Li, Photocatalytic degradation of low concentration formaldehyde and simultaneous elimination of ozone by-product using palladium modified TiO₂ films under UV₂₅₄+185 nm irradiation, *Appl. Catal. B: Environ.* 105 (2011) 220–228.
- [37] P. Fu, Characterization of Pt-TiO₂ film used in three formaldehyde photocatalytic degradation systems UV_{254nm}, O₃ + UV_{254nm} and UV₂₅₄+185nm via X-ray photoelectron spectroscopy, *Chin. J. Catal.* 35 (2014) 210–218.
- [38] B. Silva, H. Figueiredo, O.S.G.P. Soares, M.F.R. Pereira, J.L. Figueiredo, A.E. Lewandowska, M.A. Bañares, I.C. Neves, T. Tavares, Evaluation of ion exchange-modified Y and ZSM-5 zeolites in Cr(VI) biosorption and catalytic oxidation of ethyl acetate, *Appl. Catal. B: Environ.* 117–118 (2012) 406–413.
- [39] P. Bergonzo, I.W. Boyd, Low pressure photodeposition of silicon nitride films using a xenon excimer lamp, *Appl. Phys. Lett.* 63 (13) (1993) 1757–1759.
- [40] P. Fu, Photocatalytic degradation of low concentration formaldehyde and simultaneous elimination of ozone by-product using palladium modified TiO₂ films under UV₂₅₄+185nm irradiation, *Appl. Catal. B: Environ.* 105 (2011) 220–228.
- [41] S. Rong, P. Zhang, Y. Yang, L. Zhu, J. Wang, F. Liu, MnO₂ framework for instantaneous mineralization of carcinogenic airborne formaldehyde at room temperature, *ACS Catal.* 7 (2017) 1057–1067.
- [42] X. Tan, Y. Wan, Y. Huang, C. He, Z. Zhang, Z. He, L. Hu, J. Zeng, D. Shu, Three-dimensional MnO₂ porous hollow microspheres for enhanced activity as ozonaton catalysts in degradation of bisphenol A, *J. Hazard. Mater.* 321 (2017) 162–172.
- [43] H. Huang, W. Li, Destruction of toluene by ozone-enhanced photocatalysts: Performance and mechanism, *Appl. Catal. B: Environ.* 102 (2011) 449–453.
- [44] R. Sun, Q. Shi, M. Zhang, L. Xie, J. Chen, X. Yang, M. Chen, W. Zhao, Enhanced photocatalytic oxidation of toluene with a coral-like direct Z-scheme BiVO₄/g-C₃N₄ photocatalyst, *J. Alloys Compd.* 714 (2017) 619–626.
- [45] J.-J. Li, S.-C. Cai, Z. Xu, X. Chen, J. Chen, H.-P. Jia, J. Chen, Solvothermal syntheses of Bi and Zn co-doped TiO₂ with enhanced electron-hole separation and efficient photodegradation of gaseous toluene under visible-light, *J. Hazard. Mater.* 325 (2017) 261–270.
- [46] M.C. Nevárez-Martínez, M.P. Kobylánski, P. Mazierski, J. Wólkiewicz, G. Trykowski, A. Malankowska, M. Kozak, P.J. Espinoza-Montero, A. Zaleska-Medynska, Self-organized TiO₂-MnO₂ nanotube arrays for efficient photocatalytic degradation of toluene, *Molecules* 22 (2017) 564–577.
- [47] S. Weon, J. Choi, T. Park, W. Choi, Freestanding doubly open-ended TiO₂ nanotubes for efficient photocatalytic degradation of volatile organic compounds, *Appl. Catal. B: Environ.* 205 (2017) 386–392.